EAI Endorsed Transactions
on AI and Robotics
Research Article EAI.EU

Comprehensive Channel Modeling of UAV-Assisted FSO Systems under Fog, AoA Fluctuations, and Pointing Errors

Mahdi Ataee[1], Seyed Mohammad Sajad Sadough[1,*], Khadijeh Ali Mahmoodi[2]

[1]Faculty of Electrical Engineering, Shahid Beheshti University, 1983969411, Tehran, Iran
[2]Laboratoire d'Ingénierie des Systèmes de Versailles (LISV), Université Paris-Saclay, Vélizy-Villacoublay, France

Abstract

This paper investigates the outage performance of unmanned aerial vehicle (UAV)-assisted free-space optical (FSO) communication systems operating in foggy channels. The analysis jointly accounts for atmospheric turbulence, fog-induced attenuation, generalized Beckmann-distributed pointing errors (PE), and angle-of-arrival (AoA) fluctuations caused by UAV orientation jitter. A comprehensive statistical channel model is developed, from which closed-form expressions for outage probability and an analytical characterization of outage capacity are derived. The effects of receiver field-of-view (FoV) limitations and multi-UAV amplify-and-forward relaying on link reliability are also investigated. Numerical results validate the proposed analysis and reveal that AoA fluctuations impose a fundamental performance limit, resulting in an outage floor, particularly under dense fog and narrow-FoV conditions. These findings provide practical design insights for improving the reliability of UAV-assisted FSO communication systems in adverse weather environments.

Received on 15 June 2026; accepted on 04 August 2026; published on 20 August 2026

Keywords: Free-space optical (FSO) communication, unmanned aerial vehicle (UAV) relaying, optical channel modeling, fog attenuation, pointing errors, angle-of-arrival fluctuations, outage analysis

doi:10.4108/airo.13538

1. Introduction

Free-space optical (FSO) communication has emerged as a promising technology for next-generation wireless networks due to its high bandwidth, inherent security, license-free spectrum, and ease of deployment [1, 2]. Moreover, FSO systems offer low latency and immunity to electromagnetic interference, making them particularly attractive for backhaul/fronthaul links, disaster recovery, and high-capacity connections to end users [3].

However, despite these advantages, the reliability of FSO links is significantly affected by atmospheric and mechanical impairments. Weather conditions such as fog, rain, and snow attenuate and scatter the optical beam [4], while atmospheric turbulence induces temporal and spatial irradiance fluctuations [5]. In addition, transmitter–receiver misalignment, referred to as pointing error (PE), caused by building sway, vibrations, or platform motion, further degrades system performance [6]. To mitigate these impairments, several techniques have been proposed, including adaptive optics, spatial diversity, adaptive modulation and coding [7–9], and beamwidth optimization to reduce PE-induced losses [10].

Among these impairments, fog is particularly detrimental due to its severe attenuation characteristics and unpredictable occurrence. Unlike turbulence and PE, which are continuously present but moderate in impact, fog events are intermittent yet can cause drastic performance degradation [11]. In dense fog conditions, attenuation levels can be sufficiently high to completely interrupt the optical link [12]. Various approaches have been proposed to alleviate fog-induced attenuation. For instance, multi-aperture receiver systems improve performance over short distances [12], while fixed relaying configurations extend coverage but are constrained by deployment cost and lack of flexibility [13]. More

*Corresponding author. Email: s_sadough@sbu.ac.ir

recently, dual-hop and multi-hop relaying schemes that jointly mitigate fog and turbulence effects have been investigated [14, 15]. However, these approaches still face limitations in highly dynamic environments and often assume static infrastructure.

Unmanned aerial vehicles (UAVs) have recently attracted significant attention as agile relay nodes capable of enhancing connectivity and coverage without requiring permanent infrastructure [16–18]. UAV-based FSO relays can be dynamically deployed in response to adverse weather conditions, allowing flexible network reconfiguration and improved resilience [19]. Prior studies have investigated UAV-assisted FSO links under foggy conditions, including ergodic capacity analysis with PE [20] and beamwidth optimization in UAV-to-UAV optical links [21]. Despite these advances, most existing works neglect angle-of-arrival (AoA) fluctuations, which arise due to UAV orientation instability and platform dynamics. These fluctuations introduce additional randomness in the received signal and can significantly affect link reliability [17, 22]. Comprehensive UAV channel models incorporating AoA effects have also been proposed in [23–25]. More recently, AoA fluctuations have been investigated under humidity and sandstorm conditions [26] and in IRS-assisted configurations [27]. However, none of these works has jointly modeled fog attenuation, turbulence, generalized Beckmann-distributed PE, and AoA fluctuations within a unified framework.

This paper develops a unified channel model for UAV-assisted FSO communication under foggy conditions that simultaneously incorporates atmospheric turbulence, fog attenuation, generalized Beckmann-distributed PE, and AoA fluctuations. Based on this comprehensive model, a closed-form expression for the outage probability is derived, and an analytical characterization of the outage capacity is provided. In addition, the performance of multi-UAV relaying schemes in mitigating fog-induced attenuation is evaluated. The analytical results are validated through numerical simulations, which reveal that AoA fluctuations impose a fundamental performance limit, leading to an outage floor that cannot be mitigated by increasing the transmit power. It should be noted that this paper assumes quasi-stationary UAV operation, wherein the relay nodes maintain fixed hovering positions during the transmission interval. Under this assumption, UAV energy constraints do not fundamentally affect the proposed channel model, as the analysis is confined to the physical-layer propagation effects rather than the UAV's operational endurance. Aspects such as UAV mobility control, optimal relay positioning [28, 29], and energy harvesting for sustained operation [19] are treated as higher-layer system-design problems and are left for future work.

The remainder of this paper is organized as follows. Section 2 presents the system model. Section 3 derives closed-form expressions for outage probability and outage capacity. Section 4 provides numerical results, and Section 5 concludes the whole paper.

2. System Model

As illustrated in Fig. 1(a), we consider a UAV-assisted FSO communication system in which a source communicates with a destination through a multi-hop optical link consisting of both clear-air and fog-affected segments. To mitigate the severe attenuation caused by fog, N UAVs are deployed as aerial relay nodes, forming a multi-hop transmission with $N+1$ links (hops), indexed by $i \in \{0, 1, \ldots, N\}$. For analytical tractability, the UAVs are assumed to be positioned along the propagation path, and each relay operates in a fixed-gain amplify-and-forward (AF) mode. The first and last hops correspond to the source-to-UAV$_1$ and UAV$_N$-to-destination links, respectively, while the intermediate hops represent intermediate UAV-to-UAV optical links.

The system employs on-off keying (OOK) with intensity-modulation and direct-detection (IM/DD). Let d_i denote the propagation distance of the i-th hop, where d_0 represents the source-to-UAV$_1$ distance, d_i for $i = 1, \ldots, N-1$ denotes the distance between UAV$_i$ and UAV$_{i+1}$, and d_N corresponds to the UAV$_N$-to-destination distance. The total end-to-end link distance is therefore given by

$$L_{\text{total}} = \sum_{i=0}^{N} d_i. \quad (1)$$

2.1. Received Signal Model

The received signal at the i-th hop, $i \in \{0, 1, \ldots, N\}$, is given by

$$y_i = \eta h_i x_i + n_i, \quad (2)$$

where η denotes the photodetector responsivity, h_i is the channel gain of the i-th hop, $x_i \in \{0, \sqrt{2P_i}\}$ is the transmitted OOK symbol with average optical power P_i at the i-th hop, and $n_i \sim \mathcal{N}(0, \sigma_{n_i}^2)$ represents the additive Gaussian noise at the receiver of the i-th hop.

As illustrated in Fig.1 (b), the receiver lens has a finite field of view (FoV), θ_{FoV}, defining the maximum acceptance angle. The AoA, θ_a, is the deviation between the incident beam and the receiver normal. When $\theta_a \leq \theta_{\text{FoV}}$, the beam is fully collected; otherwise, the signal is lost due to beam misalignment (see Fig.1 (b)).

2.2. Optical Channel Model

The channel intensity gain of the i-th hop is modeled as [30]

$$h_i = h_{af}\, h_p\, h_{AoA}, \quad (3)$$

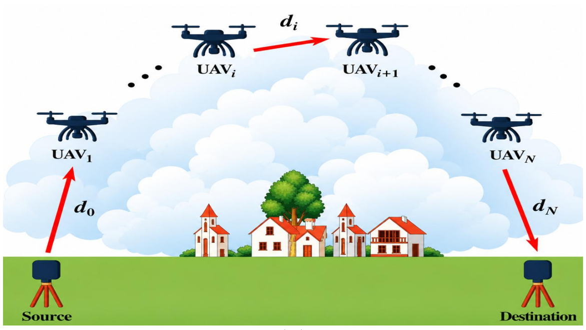

(a)

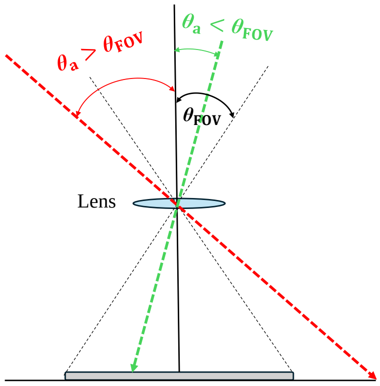

(b)

Figure 1. UAV-assisted FSO communication in foggy conditions: (a) system model, (b) received beam configuration

where h_{af} captures the combined effect of atmospheric turbulence and fog attenuation, h_p accounts for PE, and h_{AoA} represents AoA fluctuations.

1) Atmospheric Turbulence, Fog, and PE. The combined effect of atmospheric turbulence, fog, and PE is expressed as

$$h_\zeta = h_{af}\, h_p. \tag{4}$$

The joint effect of fog attenuation and atmospheric turbulence on the channel can be modeled through the probability density function (PDF) of h_{af} as [30]

$$f_{h_{af}}(h_{af}) = \frac{z^k}{\Gamma(k,0)}\left(\ln\left(\frac{1}{h_{af}}\right)\right)^{k-1} h_{af}^{z-1}, \tag{5}$$

where $0 < h_{af} \leq 1$ and $z = \frac{4.343}{\beta d}$. Here, $k > 0$ and $\beta > 0$ denote the shape and scale parameters, respectively, and $\Gamma(\cdot,\cdot)$ represents the upper incomplete Gamma function[1]. The parameter d denotes the link distance between consecutive nodes (i.e., source-to-UAV, UAV-to-UAV, or UAV-to-destination links). The parameters k and β characterize the fog conditions and depend on the fog density level. Their numerical values are specified in Section IV.

On the other hand, PE arise due to building sway, UAV displacement, and platform orientation fluctuations. These effects are modeled as the radial displacement of the optical beam footprint from the photodetector center, denoted by r, where $r^2 = x^2 + y^2$. Here, $x \sim \mathcal{N}(\mu_x, \sigma_x^2)$ and $y \sim \mathcal{N}(\mu_y, \sigma_y^2)$ represent Gaussian random variables corresponding to horizontal and vertical displacements, respectively.

For a circular beam profile, the PDF of r follows the Beckmann distribution [31], which accounts for both fixed misalignment and random jitter along the x and y axes.

The Beckmann distribution can be accurately approximated by a modified Rayleigh distribution [32]. Accordingly, the PDF of the generalized PE in the i-th hop, h_p, is given by [33]

$$h_p(r) \approx A \exp\left(-\frac{2r^2}{w_{z_{eq}}^2}\right), \quad r \geq 0, \tag{6}$$

where $A = (\mathrm{erf}(\nu))^2$ is the fraction of collected power without PE, $\nu = \frac{\sqrt{\pi}a}{\sqrt{2}w_z}$, a is the receiver diameter, and $w_{z_{eq}}^2 = w_z^2 \frac{\sqrt{\pi}A}{2\nu\exp(-\nu^2)}$ is the equivalent beamwidth. Here, $w_z \approx w_0\left[1 + \epsilon\left(\frac{\lambda z}{\pi w_0^2}\right)^2\right]^{\frac{1}{2}}$, where w_0 is the beamwidth at the transmitter ($z = 0$), $\epsilon = (1 + 2w_0^2/\rho_0^2(z))$, and $\rho_0(z) = (0.55\, C_n^2 k_w^2\, z)^{-3/5}$ denotes the coherence length, where $k_w = 2\pi/\lambda$ is the optical wavenumber.

From [32] and (6), the PDF of h_p can be expressed as

$$f_{h_p}(h_p) \simeq \frac{\varphi_m^2}{(A_m)^{\varphi_m^2}} h_p^{\varphi_m^2-1}, \quad 0 \leq h_p \leq A_m, \tag{7}$$

where $\varphi_m = \frac{w_{z_{eq}}}{2\sigma_m}$ and A_m is given by [32]

$$A_m = \exp\left(\frac{1}{\varphi_m^2} - \frac{1}{2\varphi_x^2} - \frac{1}{2\varphi_y^2} - \frac{\mu_x^2}{2\sigma_x^2\varphi_x^2} - \frac{\mu_y^2}{2\sigma_y^2\varphi_y^2}\right), \tag{8}$$

with $\varphi_x = \frac{w_{z_{eq}}}{2\sigma_x}$ and $\varphi_y = \frac{w_{z_{eq}}}{2\sigma_y}$.

Here, A_m denotes the fraction of optical power collected under generalized Beckmann-distributed PE. The total displacement spread of the pointing σ_m is given by [32]

$$\sigma_m = \left[\frac{3\mu_x^2\sigma_x^4 + 3\mu_y^2\sigma_y^4 + \sigma_x^6 + \sigma_y^6}{2}\right]^{\frac{1}{6}}. \tag{9}$$

[1] $\Gamma(a,x) = \int_x^\infty t^{a-1}e^{-t}\,dt$, with $\Gamma(a) = \Gamma(a,0)$.

The PDF of h_ζ, obtained by marginalizing over h_{af} and substituting the PDF of h_p, is [30]

$$f_{h_\zeta}(h_\zeta) = \frac{z^k \varphi_m^2 h_\zeta^{\varphi_m^2-1}}{\Gamma(k,0) A_m^{\varphi_m^2}} \int_{\frac{h_\zeta}{A_m}}^{1} \left[\ln\left(\frac{1}{h_{af}}\right)\right]^{k-1} h_{af}^{\psi-1}\, dh_{af}. \quad (10)$$

Following [23], (10) can be evaluated in closed-form as

$$f_{h_\zeta}(h_\zeta) = \frac{z^k \varphi_m^2}{\psi^k \Gamma(k,0) A_m^{\varphi_m^2}} h_\zeta^{\varphi_m^2-1} \times \left[\Gamma(k,0) - \Gamma\left(k, \psi \ln\left(\frac{A_m}{h_\zeta}\right)\right)\right], \quad (11)$$

where $\psi = z - \varphi_m^2$.

2) AoA Fluctuations. The AoA, denoted by θ_a, is modeled as a Rayleigh random variable due to fluctuations in UAV orientation and atmospheric perturbations [23]. Its PDF is expressed as

$$f_{\theta_a}(\theta_a) = \frac{\theta_a}{\sigma_\theta^2} \exp\left[-\frac{\theta_a^2}{2\sigma_\theta^2}\right], \quad \theta_a \geq 0. \quad (12)$$

As illustrated in Fig. 1 (b), if the angle of arrival of the received beam exceeds the receiver FoV, the link is interrupted. This effect is modeled through the binary random variable h_{AoA} defined as

$$h_{AoA} = \begin{cases} 1, & \theta_a \leq \theta_{\mathrm{FoV}}, \\ 0, & \theta_a > \theta_{\mathrm{FoV}}. \end{cases} \quad (13)$$

If $\theta_a > \theta_{\mathrm{FoV}}$, the optical beam falls outside the receiver aperture and is completely lost (i.e., $h_{AoA} = 0$). The corresponding PDF of h_{AoA} is given by

$$f_{h_{AoA}}(h_{AoA}) = \exp\left[-\frac{\theta_{\mathrm{FoV}}^2}{2\sigma_\theta^2}\right]\delta(h_{AoA}) + \left[1 - \exp\left(-\frac{\theta_{\mathrm{FoV}}^2}{2\sigma_\theta^2}\right)\right]\delta(h_{AoA}-1), \quad (14)$$

where $\delta(\cdot)$ denotes the Dirac delta function.

3) Comprehensive Channel Model. Although in practice a dependence between h_{AoA} and h_ζ may exist, for analytical tractability under a large value of θ_{FoV} relative to σ_θ, we can assume statistical independence between them [17]. The overall channel gain is expressed as $h_i = h_\zeta h_{AoA}$, and its PDF can be written as

$$f_{h_i}(h_i) = \int f_{h_i|h_\zeta}(h_i|h_\zeta) f_{h_\zeta}(h_\zeta) dh_\zeta. \quad (15)$$

The conditional PDF is given by

$$\begin{aligned} f_{h_i|h_\zeta}(h_i|h_\zeta) &= \frac{1}{h_\zeta} f_{h_{AoA}}\left(\frac{h_i}{h_\zeta}\right) \\ &= \frac{1}{h_\zeta}\exp\left[-\frac{\theta_{\mathrm{FoV}}^2}{2\sigma_\theta^2}\right]\delta\left(\frac{h_i}{h_\zeta}\right) \\ &+ \frac{1}{h_\zeta}\left(1 - \exp\left[-\frac{\theta_{\mathrm{FoV}}^2}{2\sigma_\theta^2}\right]\right)\delta\left(\frac{h_i}{h_\zeta} - 1\right). \end{aligned} \quad (16)$$

Substituting (16) into (15), and applying the property of Dirac delta function ($\delta(x/a) = |a|\delta(x)$), we obtain

$$\begin{aligned} f_{h_i}(h_i) &= \int f_{h_\zeta}(h_\zeta)\exp\left[-\frac{\theta_{\mathrm{FoV}}^2}{2\sigma_\theta^2}\right]\delta(h_i)\, dh_\zeta \\ &+ \int f_{h_\zeta}(h_\zeta)\left(1 - \exp\left[-\frac{\theta_{\mathrm{FoV}}^2}{2\sigma_\theta^2}\right]\right)\delta\left(h_i - h_\zeta\right) dh_\zeta, \end{aligned} \quad (17)$$

and the final expression of the PDF of the comprehensive channel model, h_i, is obtained as

$$f_{h_i}(h_i) = \exp\left[-\frac{\theta_{\mathrm{FoV}}^2}{2\sigma_\theta^2}\right]\delta(h_i) + \left[1 - \exp\left[-\frac{\theta_{\mathrm{FoV}}^2}{2\sigma_\theta^2}\right]\right] f_{h_\zeta}(h_i), \quad (18)$$

where $f_{h_\zeta}(h_i)$ is given in (11).

3. Outage Probability and Outage Capacity Analysis

In the sequel, we derive the outage probability and outage capacity for the proposed UAV-assisted FSO channel model. Unless otherwise stated, all expressions apply to an arbitrary hop indexed by i.

3.1. Outage Probability

The outage probability is defined as the probability that the instantaneous signal-to-noise ratio (SNR), $\gamma(h)$, falls below a given threshold γ_{th}. Mathematically, this is expressed as

$$P_{\mathrm{out}} = \Pr\left(\gamma(h) < \gamma_{\mathrm{th}}\right), \quad (19)$$

From (2), the instantaneous SNR can be expressed as

$$\gamma(h) = \frac{2Ph^2}{\sigma_n^2}. \quad (20)$$

Defining the average SNR as $\bar{\gamma} = \frac{2P}{\sigma_n^2}$, we can rewrite

$$\gamma(h) = \bar{\gamma} h^2. \quad (21)$$

By substituting the instantaneous SNR expression from (21) into (19), we obtain

$$P_{\mathrm{out}} = \Pr\left(\frac{2Ph^2}{\sigma_n^2} < \gamma_{\mathrm{th}}\right), \quad (22)$$

which can equivalently be written in terms of the channel gain h as

$$P_{\mathrm{out}} = \Pr(h < h_{\mathrm{th}}), \quad (23)$$

where the channel threshold h_{th} associated with the SNR threshold γ_{th} is given by

$$h_{\mathrm{th}} = \sqrt{\frac{\gamma_{\mathrm{th}}\, \sigma_n^2}{2P}}. \quad (24)$$

From (23), it is obvious that an outage occurs when the channel gain h drops below the threshold h_{th} required to sustain the required SNR, γ_{th}. Therefore, the outage probability is simply the cumulative distribution function (CDF) of h evaluated at h_{th} as

$$P_{\text{out}} = \Pr(h < h_{\text{th}}) = \int_0^{h_{\text{th}}} f_h(h)\, dh, \tag{25}$$

where $f_h(h)$ is the PDF of the comprehensive channel gain defined in (3).

By substituting the comprehensive PDF from (18) into (25), the outage probability can be expressed as

$$\begin{aligned} P_{\text{out}} &= \exp\left[-\frac{\theta_{\text{FoV}}^2}{2\sigma_\theta^2}\right] \\ &+ \left(1 - \exp\left[-\frac{\theta_{\text{FoV}}^2}{2\sigma_\theta^2}\right]\right) \int_0^{h_{\text{th}}} f_{h_\zeta}(h)\, dh, \end{aligned} \tag{26}$$

where $f_{h_\zeta}(h)$ is given in (11). The first term in (26) corresponds to the probability that the received beam falls outside the receiver FoV, leading to complete signal loss, while the second term represents the outage probability conditioned on the beam remaining within the FoV, where performance degradation is governed by fog attenuation and generalized PE. The integral in (26) can be evaluated in closed form by replacing $f_{h_\zeta}(h)$ from (11) and using the results in [23] as

$$\begin{aligned} \int_0^{h_{\text{th}}} f_{h_\zeta}(h)\, dh = \frac{-z^k}{\psi^k \Gamma(k,0)} \Bigg[& e^{-\varphi_m^2 \ln(q)}\, \Gamma\big(k, \psi \ln(q)\big) \\ & - \frac{(\psi \ln(q))^k}{w} e^{-w} \\ & - (k-1)\, \frac{(\psi \ln(q))^k}{w^k} \Gamma(k-1, w) \Bigg], \end{aligned} \tag{27}$$

where $q = A_m/\sqrt{h_{\text{th}}}$ and $w = (\varphi_m^2 + \psi)\ln(q)$. Equation (27) thus provides a closed-form expression for the outage probability under the combined effects of atmospheric turbulence, fog attenuation, generalized Beckmann-distributed PE, and AoA fluctuations.

In our multi-UAV communication scenario, the signal traverses $N+1$ hops between source and destination. The overall outage probability is thus given by [34]

$$P_{\text{out}}^{total} = 1 - \prod_{i=1}^{N+1} (1 - P_{\text{out}}^i), \tag{28}$$

where P_{out}^i denotes outage probability of the ith hop derived in (26).

3.2. Outage Capacity

In slow-fading optical channels, the system performance can also be characterized in terms of the *outage capacity*, denoted by C_{out}. This metric represents the maximum achievable transmission rate that can be supported with probability at least $(1-r)$, where r is the target outage probability. Mathematically, we have

$$\Pr(C < C_{\text{out}}) = r, \tag{29}$$

where C is the instantaneous channel capacity.

Since the instantaneous SNR $\gamma(h)$ is a random variable, the corresponding capacity C is also random. Therefore, the outage probability in (29) can equivalently be expressed as

$$r = \int_0^{C_{\text{out}}} f_C(C)\, dC = F_C(C_{\text{out}}), \tag{30}$$

where $f_C(C)$ and $F_C(C)$ denote the PDF and CDF of the instantaneous capacity, C, respectively.

Using the Shannon capacity formula together with the SNR expression in (21), the instantaneous capacity is given by

$$C = B \log_2[1 + \gamma] = B \log_2\left[1 + \bar{\gamma} h^2\right], \tag{31}$$

where B is the channel bandwidth.

Because C is a deterministic function of the random variable h, we can write $C = g(h)$. By applying the standard transformation of random variables, the CDF of C can be expressed in terms of the CDF of h as

$$F_C(C) = F_h\big(g^{-1}(C)\big), \tag{32}$$

where $g(h)$ is defined in (31), and its inverse is given by

$$h = g^{-1}(C) = \sqrt{\frac{2^{C/B} - 1}{\bar{\gamma}}}. \tag{33}$$

By substituting (33) into the closed-form CDF of h derived from (27), the CDF of the instantaneous capacity C can be expressed as

$$\begin{aligned} F_C(C) = \frac{z^k}{\psi^k \Gamma(k,0)} \Bigg[& - e^{-\varphi_m^2 \ln(q)}\, \Gamma\big(k, \psi \ln(q)\big) \\ & + w^{-1} (\psi \ln(q))^k e^{-w} \\ & + (\psi \ln(q))^k (k-1) w^{-(k-1)} \Gamma(k-1, w) \Bigg], \end{aligned} \tag{34}$$

where $q = A_m/\sqrt{2^{C/B} - 1/\bar{\gamma}}$, and $w = \left(\varphi_m^2 + \psi\right)\ln(q)$.

For any desired outage probability r, the corresponding outage capacity C_{out} can be determined by substituting (34) into (30), which yields

$$\begin{aligned} r = F_C(C_{\text{out}}) = \frac{z^k}{\psi^k \Gamma(k,0)} \Bigg[& - e^{-\varphi_m^2 \ln(q_{\text{out}})}\, \Gamma\big(k, \psi \ln(q_{\text{out}})\big) \\ & + w_{\text{out}}^{-1} (\psi \ln(q_{\text{out}}))^k e^{-w_{\text{out}}} \\ & + (\psi \ln(q_{\text{out}}))^k (k-1) w_{\text{out}}^{-(k-1)} \Gamma(k-1, w_{\text{out}}) \Bigg], \end{aligned} \tag{35}$$

Table 1. System configuration and parameters

Parameter (unit)	Variable	Value
Responsivity	η	0.5
Noise standard deviation	σ_n	10^{-7}
Receiver radius (cm)	r_a	10
FSO wavelength (nm)	λ	1550
Optical transmitted power (dBm)	P_t	16
Refraction index ($m^{-2/3}$)	$C_n^2(0)$	5×10^{-14}, 2×10^{-13}
Link length (km)	L_{total}	19–22
Standard deviation	σ_m	0.1
UAV altitude (m)	H_{uav}	50–350
Nominal beamwidth (m)	w_Z	2.5
Optimum beamwidth (m)	w_{opt}	0.6×10^{-3}
Receiver FoV (mrad)	θ_{FoV}	30
Beam deviation variance (mrad)	σ_θ	10
Fog distribution parameters	Light fog	$k = 2.32$, $\beta = 13.12$
	Moderate fog	$k = 5.49$, $\beta = 12.06$
	Thick fog	$k = 6.00$, $\beta = 23.00$
	Dense fog	$k = 36.05$, $\beta = 11.91$

where $q_{\text{out}} = A_m/\sqrt{2^{C_{\text{out}}/B} - 1/\bar{\gamma}}$, and $w_{\text{out}} = \left(\varphi_m^2 + \psi\right)\ln(q_{\text{out}})$.

Although (35) does not explicitly produce yet a closed-form expression for C_{out} as a function of r, it provides a complete analytical characterization from which C_{out} can be efficiently obtained by numerical inversion, as addressed in the following.

4. Numerical Results and Discussion

This section presents numerical results to validate the analytical expressions derived earlier. Unless otherwise specified, the system and channel parameters are provided in Table 1. These parameter values are adopted from established prior works in the literature to ensure fair comparison and consistency with existing studies. We assume $N = 4$ UAVs with identical hop distances $d_i = 0.4$ km, $i = 0, 1, \ldots, N$, which represents a nominal inter-node separation enabling reliable FSO transmission with acceptable outage performance under the considered system parameters.

Fig. 2 illustrates the effect of AoA fluctuations on the outage performance of the proposed system. It can be observed that for values of σ_θ greater than 4.5 mrad, neglecting the AoA effect in the system model leads to a considerable deviation in the computed outage probability. For instance, at $P_t = 20$ dBm and $\sigma_\theta = 5$ mrad, $P_{\text{out}}^{(N=4)} = 8 \times 10^{-3}$ for the case without considering AoA, while it is $P_{\text{out}}^{(N=4)} = 9 \times 10^{-3}$ for the case where AoA is considered, the resulting discrepancy is approximately 12%, indicating a modest but non-negligible increase in outage probability when AoA fluctuations are properly accounted for.

The figure also compares results for three different transmitted power levels, highlighting that higher transmit power reduces the sensitivity of the system to AoA fluctuations. For instance at $\sigma_\theta = 5$ mrad,

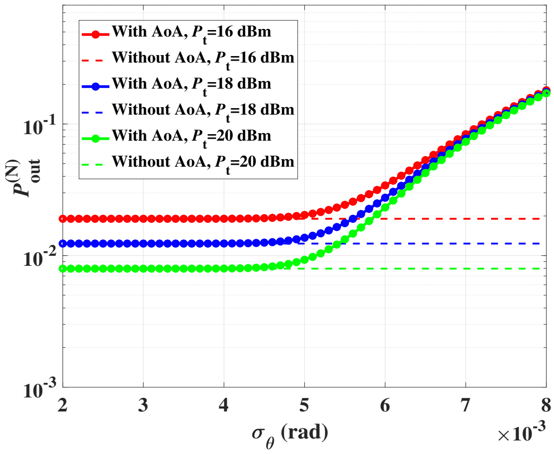

Figure 2. Outage probability versus σ_θ for different values of transmitter power

when $P_t = 16$ dBm, we observe $P_{\text{out}}^{(N=4)} = 2 \times 10^{-2}$ while it reduces to $P_{\text{out}}^{(N=4)} = 13 \times 10^{-3}$, and $P_{\text{out}}^{(N=4)} = 9 \times 10^{-3}$, for $P_t = 18$ dBm, and $P_t = 20$ dBm, respectively. According to these results, more precise designs can be carried out using the provided closed-form formula of outage performance, in which the effect of σ_θ is also included.

Fig. 3 illustrates the outage probability as a function of the transmitter power for different values of θ_{FoV}. It is observed that increasing θ_{FoV} improves system performance, as a wider FoV reduces the probability of link interruption caused by AoA fluctuations. Moreover, increasing the transmitter power significantly reduces the outage probability in the low- and moderate-power regimes. However, beyond approximately $P_t \approx$ 30–35 dBm, the outage probability exhibits a saturation behavior and approaches a floor. This performance floor arises due to AoA-induced link interruptions, which cannot be mitigated by simply increasing the transmit power. In contrast, the benchmark model, which does not account for AoA fluctuations, shows a continuous improvement with increasing transmit power and does not exhibit such a saturation effect.

Fig. 4 illustrates the impact of PE and fog on outage capacity. Under light fog, PE significantly affects performance: reducing the PE spread from $\sigma_m = 0.31$ to $\sigma_m = 0.22$ increases the outage capacity at $P_t = 25$ dBm from 17.2 Gbps to 19.7 Gbps. In contrast, under moderate fog, capacity is much lower—0.09 Gbps and 0.17 Gbps for $\sigma_m = 0.31$ and $\sigma_m = 0.22$, respectively—indicating that fog-induced attenuation dominates, reducing the relative impact of PE.

Fig. 5 shows the variation of outage probability with transmitted power for different numbers of UAVs used as relays, assuming a total link distance of $L_{\text{total}} =$ 2 km. Results are presented for LoS transmission ($N =$

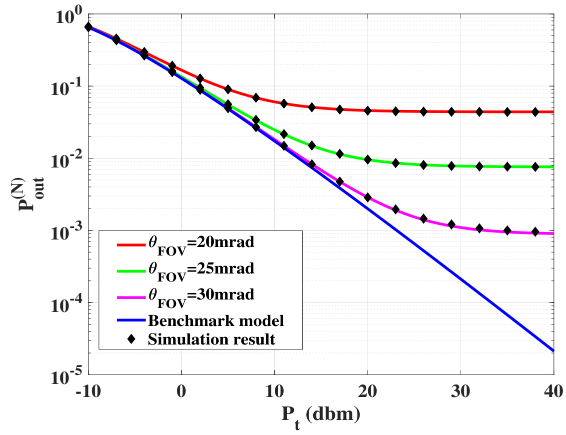

Figure 3. Outage probability versus transmitter power for different values of θ_{FOV}

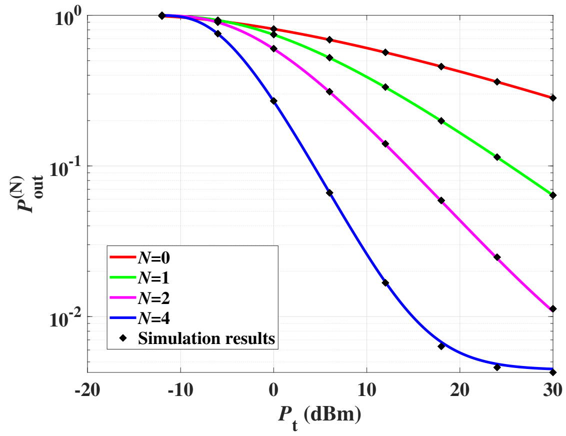

Figure 5. Outage probability versus transmitted power for different numbers of UAVs

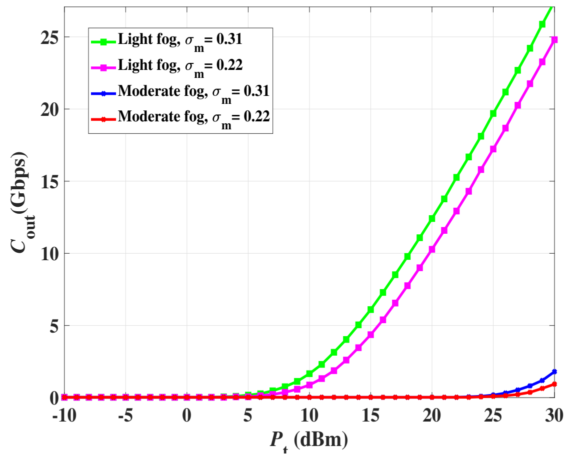

Figure 4. Outage capacity versus transmitted power for different fog and PE conditions

0) and for 1, 2, and 4 UAV-assisted links. A substantial performance improvement is observed compared to LoS transmission, particularly at moderate and high transmit power levels. For instance, at $P_t = 15$ dBm, the outage probability is approximately equal to $P_{\text{out}}^{(N)} = 0.5$, 0.23, 0.09, and 0.01 for 0, 1, 2, and 4 UAVs, respectively. Moreover, we observe that the analytical curves closely match the Monte Carlo simulation results obtained using 10^6 channel realizations, confirming the accuracy of the derived expressions. The results highlight the effectiveness of multi-hop UAV relaying in mitigating fog-induced losses and turbulence fading.

5. Conclusion

This paper analyzed the outage performance of UAV-assisted FSO communication systems over foggy channels while jointly accounting for atmospheric turbulence, fog attenuation, generalized Beckmann-distributed PE, and AoA fluctuations. A comprehensive statistical channel model was developed, enabling the derivation of closed-form expressions for the outage probability and an analytical characterization of the outage capacity, which were validated through simulations. The results demonstrate that link reliability remains acceptable under light and moderate fog conditions, whereas thick and dense fog lead to severe attenuation and a significant increase in outage probability. Furthermore, AoA fluctuations were shown to impose a critical performance limitation, particularly under narrow FoV conditions, resulting in an outage floor that cannot be mitigated by increasing transmit power. In addition, multi-UAV relaying was found to effectively alleviate fog- and PE-induced degradations, thereby improving end-to-end system reliability. These findings provide useful insights for the design of robust UAV-assisted FSO systems operating in adverse weather environments. It is worth noting that the emergence of an AoA-induced outage floor is qualitatively consistent with trends reported in prior UAV-FSO studies incorporating AoA effects [22–24, 26], which similarly observe a saturation in link reliability at high transmit power once orientation-induced misalignment is modeled. However, a direct quantitative comparison is not performed here, as these works differ in system parameters (e.g., link geometry, fog/turbulence models, and FoV configuration), which precludes a fair numeric benchmark; the present comparison is instead confined to the case with AoA versus the benchmark model without AoA fluctuations, in order to isolate the specific contribution of AoA modeling.

References

[1] Wang F, Qiu C, Zhang M, Hu G. Free-Space Optical Communication Based on Mode Diversity Reception

Using a Nonmode Selective Photonic Lantern and Equal Gain Combining. IEEE Photonics Journal. 2023;15(1):1-7.

[2] Saber MJ, Sadough SMS. On secure free-space optical communications over Málaga turbulence channels. IEEE Wireless Communications Letters. 2017;6(2):274-7.

[3] Alimi IA, Monteiro PP. Revolutionizing Free-Space Optics: A Survey of Enabling Technologies, Challenges, Trends, and Prospects of Beyond 5G Free-Space Optical (FSO) Communication Systems. Sensors. 2024;24(24). Available from: https://www.mdpi.com/1424-8220/24/24/8036.

[4] Ghanbari M, Jahed MS, Sajad Sadough SM. On the Interaction Between Meteorological Conditions and Performance Optimization in MISO Free-Space Optical Communication. In: 2023 31st International Conference on Electrical Engineering (ICEE); 2023. p. 479-83.

[5] Andrews LC, Phillips RL. Laser beam propagation through random media. Laser Beam Propagation Through Random Media: Second Edition. 2005.

[6] Trung HD, Pham AT, et al. Pointing error effects on performance of free-space optical communication systems using SC-QAM signals over atmospheric turbulence channels. AEU-International Journal of Electronics and Communications. 2014;68(9):869-76.

[7] Liang Y, Su X, Wang L, Wang J. Free-Space Adaptive Optical Communication Systems Against Atmospheric Turbulence and Device Vibrations. In: Conference on Lasers and Electro-Optics. Optica Publishing Group; 2020. p. JTu2E.16.

[8] Nouri H, Uysal M. Adaptive MIMO FSO Communication systems with spatial mode switching. Journal of Optical Communications and Networking. 2018;10(8):686-94.

[9] Safi H, Sharifi AA, Dabiri MT, Ansari IS, Cheng J. Adaptive channel coding and power control for practical FSO communication systems under channel estimation error. IEEE Transactions on Vehicular Technology. 2019;68(8):7566-77.

[10] Jahed MS, Ghanbari M, Sadough SMS. Bit Error Rate Analysis for a Mixed Underwater OWC-FSO Relaying System in the Presence of Pointing Error. In: 2023 31st International Conference on Electrical Engineering (ICEE); 2023. p. 512-6.

[11] Esmail MA, Fathallah H, Alouini MS. Channel modeling and performance evaluation of FSO communication systems in fog. In: 2016 23rd International Conference on Telecommunications (ICT); 2016. p. 1-5.

[12] Rahman Z, Zafaruddin SM, Chaubey VK. Performance of Opportunistic Beam Selection for OWC System Under Foggy Channel with Pointing Error. IEEE Communications Letters. 2020;24(9):2029-33.

[13] Esmail MA, Fathallah H, Alouini MS. Outage Probability Analysis of FSO Links Over Foggy Channel. IEEE Photonics Journal. 2017;9(2):1-12.

[14] Rahman Z, Shah TN, Zafaruddin SM, Chaubey VK. Performance of Dual-Hop Relaying for OWC System Over Foggy Channel With Pointing Errors and Atmospheric Turbulence. IEEE Transactions on Vehicular Technology. 2022;71(4):3776-91.

[15] Rahman Z, Zafaruddin SM, Chaubey VK. Multihop Optical Wireless Communication Over $\mathcal{F}$-Turbulence Channels and Generalized Pointing Errors With Fog-Induced Fading. IEEE Photonics Journal. 2022;14(5):1-14.

[16] Ghanbari M, Ataee M, Sadough SMS. Outage performance analysis for UAV-based mixed underwater-FSO communication under pointing errors. In: 2022 4th West Asian Symposium on Optical and Millimeter-wave Wireless Communications (WASOWC). IEEE; 2022. p. 1-5.

[17] Dabiri MT, Sadough SMS. Optimal placement of UAV-assisted free-space optical communication systems with DF relaying. IEEE Communications Letters. 2019;24(1):155-8.

[18] Mahmoodi KA, Elamassie M, Uysal M. Operation Altitude Optimization of Solar-Powered Rotary-Wing UAVs for FSO Backhauling. In: 2023 International Balkan Conference on Communications and Networking (BalkanCom); 2023. p. 1-6.

[19] Uysal M, Mahmoodi KA, Elamassie M. Toward Self-Sustainable Airborne Communication Networks: Comprehensive Modeling and Analysis of Energy Consumption and Harvesting. IEEE Vehicular Technology Magazine. 2026;21(2):142-51.

[20] Jung KJ, Nam SS, Alouini MS, Ko YC. Ergodic Capacity Analysis of UAV-Based FSO Links Over Foggy Channels. IEEE Wireless Communications Letters. 2022;11(7):1483-7.

[21] Yang R, Han J, Liang L, Li R, Zhou Y. Joint channel model for fog and atmospheric turbulence and performance analysis of unmanned aerial vehicles' free-space optical communication. Optical Engineering. 2023 jan;62:016104.

[22] Xu M, Xu G, Dong Y, Wang W, Zhang Q, Song Z. UAV-assisted FSO communication system with amplify-and-forward protocol under AOA fluctuations: A performance analysis. China Communications. 2023;20(11):111-30.

[23] Dabiri MT, Sadough SMS, Khalighi MA. Channel modeling and parameter optimization for hovering UAV-based free-space optical links. IEEE Journal on Selected Areas in Communications. 2018;36(9):2104-13.

[24] Dabiri MT, Sadough SMS, Ansari IS. Tractable optical channel modeling between UAVs. IEEE Transactions on Vehicular Technology. 2019;68(12):11543-50.

[25] Xu G, Zhang N, Xu M, Xu Z, Zhang Q, Song Z. Outage Probability and Average BER of UAV-Assisted Dual-Hop FSO Communication With Amplify-and-Forward Relaying. IEEE Transactions on Vehicular Technology. 2023;72(7):8287-302.

[26] Salih Mohammed Gismalla M, Al-Dharrab SI, Alawsh SA, Muqaibel AH. Performance Analysis of Multi-Hop UAVs Using FSO Communications Under Humidity and Sandstorms Conditions. IEEE Open Journal of the Communications Society. 2024;5:6987-7001.

[27] Sharma P, R S. Performance Analysis of UAV-Based IRS-Assisted FSO Communication Systems. In: 2025 IEEE 101st Vehicular Technology Conference (VTC2025-Spring); 2025. p. 1-6.

[28] Yang Y, Liao L, Yang H, Li S. An Optimal Control Strategy for Multi-UAVs Target Tracking and Cooperative Competition. IEEE/CAA Journal of

Automatica Sinica. 2021;8(12):1931-47.

[29] Moshayedi AJ, Roy AS, Karan U, Zhang M, Bassir D. An Integrated Beetle Antennae Search–Enabled Navigation Framework for Omnidirectional AGVMobile Robots in Unknown Environments. EAI Endorsed Transactions on AI and Robotics. 2026;5. Available from: https://hal.science/hal-05550335.

[30] Esmail MA, Fathallah H, Alouini MS. On the Performance of Optical Wireless Links Over Random Foggy Channels. IEEE Access. 2017;5:2894-903.

[31] Alaouni MS, Simon MK. Digital communications over fading channels. Wiley; 2005. .

[32] Boluda-Ruiz R, García-Zambrana A, Castillo-Vázquez C, Castillo-Vázquez B. Novel approximation of misalignment fading modeled by Beckmann distribution on free-space optical links. Optics express. 2016;24(20):22635-49.

[33] Farid AA, Hranilovic S. Outage capacity optimization for free-space optical links with pointing errors. Journal of Lightwave technology. 2007;25(7):1702-10.

[34] Papoulis A. Probability, Random Variables, and Stochastic Processes. vol. 4th ed. McGraw-Hill; 2002. .